




# Design and analysis of response threshold of energy selective surface based on serial LC circuits

Ning Hu<sup>1</sup> , Xi Zhu<sup>1</sup>, He Wang<sup>1</sup>, Haojie Yin<sup>1</sup> and Yanlin Xu<sup>2</sup>

<sup>1</sup>Information Engineering University, Zhengzhou, China and <sup>2</sup>College of Electronic Science and Technology, National University of Defense Technology, Changsha, China

## Research Paper

**Cite this article:** Hu N, Zhu X, Wang H, Yin H, Xu Y (2024) Design and analysis of response threshold of energy selective surface based on serial LC circuits. *International Journal of Microwave and Wireless Technologies* **16**(7), 1181–1186. <https://doi.org/10.1017/S1759078724000771>

Received: 13 January 2024  
Revised: 27 May 2024  
Accepted: 10 June 2024

### Keywords:

energy selective surface; high intensity radio frequency (HIRF) protection; response threshold; serial LC circuits

**Corresponding author:** Yanlin Xu;  
Email: [13298656824@163.com](mailto:13298656824@163.com)

### Abstract

This paper presents a method to design the response threshold (RT) of energy selective surface (ESS) based on series LC circuits (SLC\_based\_ESS). A simple SLC\_based\_ESS structure composed of metal strips and PIN diodes is used for demonstration. According to our research, the RT is rarely related to the geometry parameters of unit cells. By contrast, the RT could be designed by introducing auxiliary structures (ASs) to SLC\_based\_ESS arrays. With the AS, the induced currents on diodes are enhanced and thus RT is greatly reduced. Prototypes are fabricated and measured under different power levels. The results agree well with simulations, proving an effective design of RT by the proposed method.

### Introduction

Energy selective surface (ESS) is a kind of periodic structures designed for high intensive radio frequency (HIRF) protection [1–3]. The transmission coefficient of ESS is power-dependent. Specifically, low-power signals could propagate through ESS, but those high-power ones are shielded/reflected.

In recent years, ESS has aroused strong interests of researchers and various types of ESS are proposed. In [4], an L-band ESS is designed with metal strips loaded with PIN diodes. In [5–7], bandpass ESSs in S band are designed with diodes implemented on square slot structures. Furthermore, ultra-wideband ESSs are realized with multi-layer metallic patterns [9, 10] and 3D structures [11]. A design method based on a double resonance concept is proposed in [12, 13], with which ESSs with low insertion loss and high shielding effectiveness are realized. The proposed method is also applied in the design of multiband ESS [14]. Furthermore, an ESS with absorptive band is proposed [15] and a novel waveguide ESS is designed and analyzed with high impedance surface theory [16]. Besides, an energy selective antenna is also proposed in [17] where adaptive protection against HIRF is achieved through integrated antenna technology.

Despite the significant progress in the structure design of ESS, the research in the nonlinear response to the field intensity of ESS is rarely explored. The response threshold (RT), the certain threshold on which ESSs are triggered on by incident waves and change its transmission state, is a critical factor [8]. If the RT is too large, ESS cannot be triggered on even the electric equipment has been damaged by HIRF. On the contrary, ESS would block the working signals if RT is too small. Considering that ESSs are directly triggered by the incident waves to achieve fast response and no external control is used [12], the design of RT could be challenging. In [18], Yang et al. proposed a method to design the RT by changing the types of diodes used in ESS. However, this method is not feasible when a certain type of diode is selected due to other reasons.

In our previous works [19], the physical mechanism of the RT of ESS is explored and a method to design the RT of ESS based on parallel LC resonance circuits (PLC\_based\_ESS) is proposed. The results of simulations and experiments show that the RT of this kind of ESSs is closely related to the quality factor  $Q_p$  of the corresponding equivalent-circuit model (ECM). By changing the geometry parameters of unit cells,  $Q_p$  can be changed. The larger the  $Q_p$ , the smaller the RT. However, this method may not work for the design of the RT of ESS based on serials LC resonance circuits (SLC\_based\_ESS) because of the distinction of circuit topology.

This paper aims at the exploration of physical mechanism of the RT of SLC\_based\_ESS and presenting effective design approaches. To the best of our knowledge, this is the first attempt to propose a design method of the RT of SLC\_based\_ESS.

The rest of the paper is arranged as follows: In Section II: Simulation and analysis of RT of SLC\_based\_ESS, various parameters are explored with respect to unit cells and arrays of SLC\_based\_ESS. A specific structure is used for demonstration and a method is proposed to design RT. The ECM and distribution of currents and electric field are adopted for analysis. Then prototypes are fabricated and measured in in Section III: Fabrication and experiments. Finally, the conclusions are draw in Section IV: Conclusion.

### Simulation and analysis of RT of SLC\_based\_ESS

#### Simulation and analysis of unit cells

In the design of SLC\_based\_ESSs, an SLC resonance circuit is used to generate a stopband for high-power signals. As the stopband moves away for low-power signals, the incident waves are able to propagate. A good example of SLC\_based\_ESS is provided in [4] and is adopted for demonstration in this paper. This proposed structure in [4] is composed of metal strips in serial with PIN diodes, seen in Figure 1(a). The ECM of the design is simple where the metal strip is modeled as an inductor  $L_s$ , and the diode is modeled as a capacitor  $C_{diode}$  (0.15 pF) in OFF state and an inductor  $L_{ON}$  (0.75 nH) in serial with a resistor  $R_s$  (1.5  $\Omega$ ) in ON state, as shown in Figure 1(b). The metal strips-based ESS (MSESS) works in L band and below.

A commercial software CST MWS (2021) is used for simulations in the paper. The property of MSESS is firstly analyzed with unit cells, which is regarded as infinite arrays. Figure 2(a) reveals the transmission coefficient of the MSESS under different conditions. For low-power signals, the diode is OFF and the SLC circuit resonates at about 6.1 GHz, and the structure is wave-transparent in the working band. By contrast, the structure becomes inductive when diodes are turned on by high-power signals. Therefore, signals are blocked in the working band. Because PIN diodes are voltage-controlled devices, the induced voltage on the diodes could be adopted to evaluate the RT of PLC\_based\_ESS. However, the SLC resonance is more closely related to the currents. Therefore, the induced currents are used to evaluate the RT of SLC\_based\_ESS in this paper. Obviously, ESS with larger induced currents are easier to be triggered on and the RT is lower. By contrast, RT would increase if the induced currents are small. As shown in Figure 2(b), the peak of induced currents on the diodes occurs at the resonance frequency of the ECM. This is also valid when the geometry parameters vary. Furthermore, the induced currents are calculated under different geometry parameters,  $w$  and  $g$ . As seen in Figure 3, the increasing in  $w$  and  $g$  leads to a rise in the peak of induced currents. The relationship between  $L_s$ ,  $w$ , and  $g$  can be indicated in a simple form [20] as

$$L_s \propto (P - g)/w. \tag{1}$$

Obviously,  $L_s$  is negatively related to both  $w$  and  $g$ . A more accurate analytic formula of the structure could be found in [21], according to which  $L_s$  is calculated to be 0.36 nH at this paper. Furthermore, the quality factor is obtained with

$$Q_s = \frac{1}{r} \sqrt{\frac{C_{diode}}{L_s}} \tag{2}$$

where  $r$  is the ohmic loss in the circuit ( $r$  is not shown in the figure of the ECM for simplicity and can be regarded in serial with  $L_s$ ). Therefore, the peak of induced currents also rises with  $Q_s$ , which is similar to PLC\_based\_ESS. However, this mechanism is only valid at the resonant frequency range. By contrast, the variation on geometry parameters only causes slight influence on induced currents in the working band of MSESS, which lies on the non-resonant frequency range. Therefore, the design method of RT for PLC\_based\_ESS, namely by changing the value of quality factor of ECM or geometry parameters of unit cells, may not be applicable at this time.

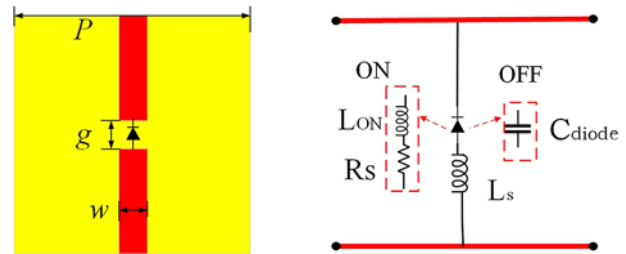


Figure 1. Geometry parameters and the ECM of the MSESS. The parameters are set as  $P = 6$  mm,  $g = 0.8$  mm,  $w = 1$  mm.

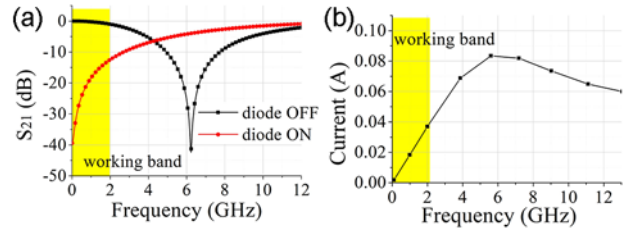


Figure 2. (a) The transmission coefficient of the MSESS under different power levels and (b) the induced currents on diodes under low-power signals.

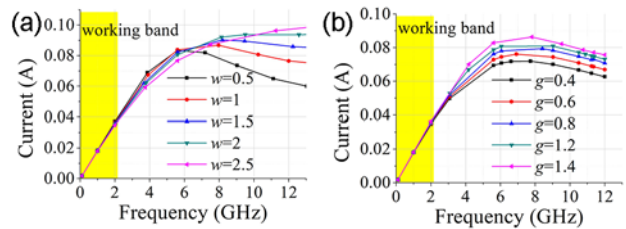


Figure 3. The induced currents on the diodes under different parameters: (a)  $w$  varies from 0.5 mm to 2.5 mm and (b)  $g$  varies from 0.4 mm to 1.4 mm.

#### Simulation and analysis of arrays

Since the induced currents are not sensitive to the variation on  $Q_s$ , a possible method is to introduce some additional auxiliary structures (ASs) and enhance the currents on diodes in the non-resonant frequency range. The AS is not required for the design of the electromagnetic (EM) response of ESS, which is added as an extra part of ESS to design RT. However, adding AS to the unit cells of ESS may cause a significant influence on the transmission performance of ESS, hence the AS is introduced to the ESS arrays. The ECM of an ESS array including  $m \times n$  unit cells could be obtained with simple processes. Shown in Figure 4, there are  $m$  rows and  $n$  columns in the array. The impedance of each unit cell is represented as  $Z_{ESS} = Z_s + Z_c$ , where  $Z_s$  and  $Z_c$  indicate the self impedance and mutual impedance of each unit cell, respectively. Then the impedance of each column of the array  $Z_{col}$  could be calculated by

$$Z_{col} = Z_s + Z_c + \dots + Z_s + Z_c + Z_s = mZ_s + (m - 1)Z_c = (m - 1)Z_{ESS} + Z_c. \tag{3}$$

The impedance of the ESS array  $Z_{ESSA}$  is obtained by

$$Z_{ESSA} = Z_v || Z_v \dots || Z_v = Z_{col}/n = (m - 1)Z_{ESS}/n + Z_c/n. \tag{4}$$

Obviously, as  $m$  and  $n$  increases,  $Z_{ESSA}$  gradually approaches  $Z_{ESS}$ , indicating that an ESS array with finite unit cells could be analyzed with the same ECM as the unit cell (infinite array) approximately.

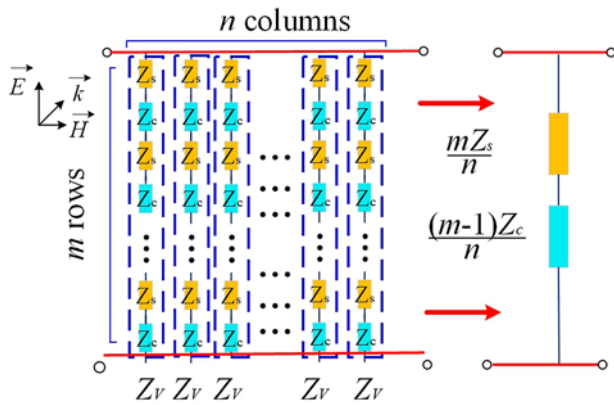


Figure 4. The ECM of an ESS array with  $m \times n$  unit cells.

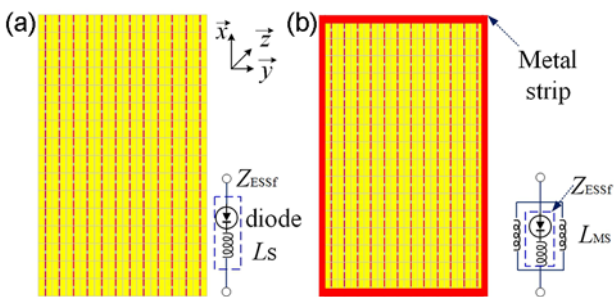


Figure 5. The ECM of the MESS array (a) without and (b) with AS (metal strips).

As for the MESS, four metal strips are introduced to the MESS array as AS, shown in Figure 5. The AS acts as an inductor  $L_{MS}$ , and thus the ECM of the MESS array turns to a PLC circuit despite that the ECM of unit cell remains SLC circuits. Because  $L_{MS}$  is much larger than  $L_s$ , the PLC resonance of the MESS array occurs at a much lower frequency range than SLC resonance of the single unit cell. Therefore, the induced currents are greatly enhanced during the operating frequency band due to the AS. Compared to the array without AS, the RT is supposed to be significantly reduced. By introducing AS into ESS design, the circuit topology of SLC\_based\_ESSs arrays could be changed from SLC to PLC, thus effectively changing the RT.

**Demonstration and verification**

An MESS array including  $16 \times 32$  unit cells is investigated with full-wave simulations for verification (although it is better to choose a larger dimension, much more computing resources are required). A plane wave (10 V/m) is used as excitation and open boundary condition is applied at  $x$ ,  $y$ , and  $z$  direction. As shown in Figure 6, the induced currents on the diodes of the MESS array, with and without AS, are calculated for verification at a normal incidence. Apparently, the currents on the array with AS are generally enhanced compared to the one without AS in the operating band as expected. Besides, it can be seen that the induced currents vary with the positions of diodes in the array. This non-uniform distribution of currents is caused by the discontinuity of impedance on the boundary. What's more, the induced currents also vary with frequency and there are several peaks caused by the resonance of the arrays.

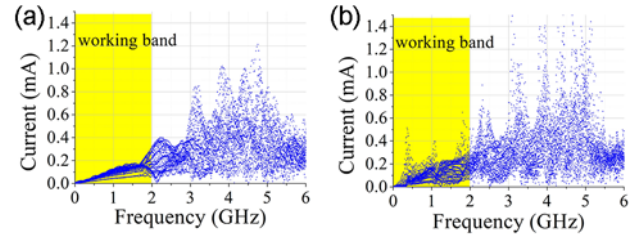


Figure 6. The induced currents on the diodes of the MESS arrays (a) without and (b) with AS.

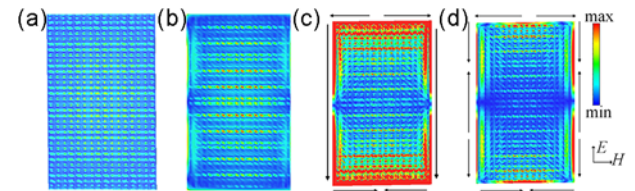


Figure 7. The distribution of electric field of the MESS arrays (a) without AS at 1.3 GHz, (b) with AS at 1.3 GHz, (c) with AS at 0.36 GHz, and (d) with AS at 1.1 GHz.

The distribution of electric field is calculated for verification. The distributions of electric field at 1.3 GHz (which is also the frequency for high-power signal measurement) with and without AS are compared, as seen in Figures 7(a) and 7(b). Obviously, the electric field on the MESS arrays is not uniform due to the impedance discontinuity on the boundary. Specially, the phenomenon is more significant when AS is added. The non-uniform distribution of electric field on the array is supposed to make the diodes easier to be triggered on. Once the diodes at positions with larger induced currents are turned-on, the impedance of diodes become smaller and thus the currents are further enhanced. As a result, the adjacent diodes would also be turned on.

Notably that two peaks of induced currents occur at 0.36 GHz and 1.1 GHz on the MESS array with AS, the electric field and surface current at these two peaks are investigated, as shown in Figures 7(c) and 7(d). Obviously, strong electric field is excited at the AS and the unit cells near two ends of the array at 0.36 GHz. At the same time, strong surface currents are also excited along AS. The distribution of electric field and surface current indicate that a strong resonance is excited on the AS, which contributes to the rise of the induced currents on diodes. The distribution of electric field and currents at 1.1 GHz is similar to the second-order resonance at 0.36 GHz.

**Fabrication and experiments**

**Experimental setup**

To verify our analysis, two prototypes are fabricated in which PIN diodes BAP-51-02 from NXP semiconductor are soldered on the F4BME substrate (which has a permittivity of 2.2 and dielectric loss tangent of 0.007) with a thickness of 0.1 mm, as seen in Figure 8 (the AS around the large one are already removed before taking pictures). The dimension of two prototypes is 8 mm  $\times$  16 mm (DUT1) and 300 mm  $\times$  300 mm (DUT2), respectively. DUT1 is used for a better verification of simulations while the DUT2 for a standard measurement. The geometry parameters of unit cells of both prototypes are the same. To explore the influence of AS on the RT and

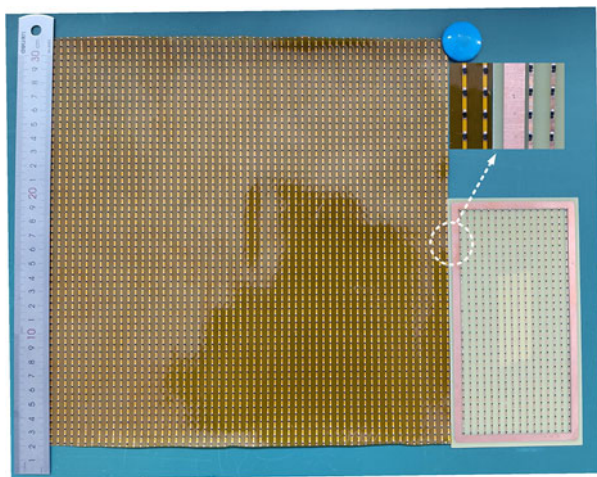


**Figure 8.** The two prototypes of MESS with a dimension of 8 mm × 16 mm (DUT1) and 300 mm × 300 mm (DUT2), respectively.

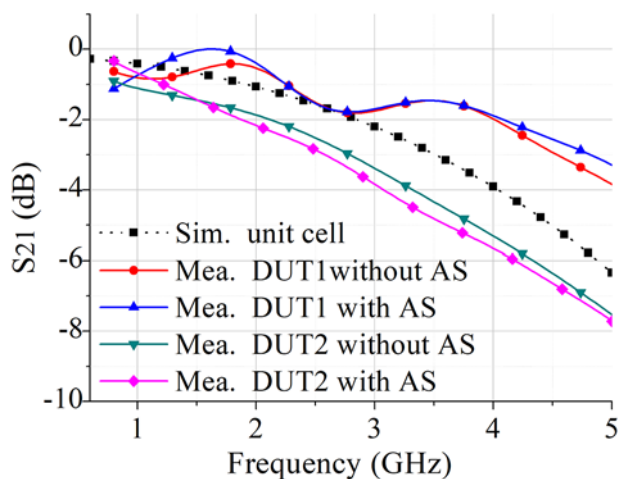


**Figure 9.** The transmission coefficient of two MESS prototypes with and without AS for low power signals (Sim: simulation results, Mea: measured results).

transmission performance of the prototypes, the experiments are conducted as following steps:

- (i) Low-power signal measurements with AS;
- (ii) High-power signal measurements with AS;
- (iii) Remove the AS and repeat (i) and (ii).

Obviously, only two prototypes are required and each prototype is tested repeatedly under different conditions. The results with and without AS from the same prototypes are compared to eliminate the measurement errors. For low-power signals, the transmission coefficient is measured in an anechoic chamber with a vector network analyzer (from Ceyear AV3672E). The DUTs are placed in the central of an absorbing wall with two broadband horn antennas on the front and back, respectively. For high-power signals, a high-power source is used to generate high-power illumination, and an oscilloscope is applied to monitor the field intensity. The experiments are conducted at a microwave anechoic chamber and the ESS prototype is mounted on the window of a shielding box. The detailed experimental setup is illustrated in our previous works [9, 12] and not illustrated in this paper.

### Low-power signal measurements

For the low-power signals, the two prototypes are measured under a normally incident plane wave and the transmission coefficient is shown in Figure 9. Interestingly, there are obvious fluctuations with frequencies on the transmission coefficient for DUT1 with and without AS. The fluctuations mainly contribute to the small dimension of DUT1 and unexpected resonance occurs at the test window. However, such a fluctuation is smaller than 1 dB and could be ignored in the measurements for high power signals. Regarding the size of the DUT1, which is too small to be considered as an infinite array in the experimental frequency range, the measurement results of transmission coefficient for DUT1 is not reliable. Since the focus of this paper is the RT of ESS, DUT1 is fabricated and measured to explore the relationship between the size of AS and RT. There is a better agreement on the results of measurements and simulations for DUT2. The measured transmission coefficient is almost 1 dB smaller than the simulations, and the difference becomes larger with frequency. There are two main reasons. Firstly, the equivalent capacitor  $C_{diode}$  used in the simulations is 0.15 pF (which is a typical value for reference). However,  $C_{diode}$  varies in a certain range, which introduces errors and this kind of error would increase with frequency, shown in Figure 10(a). Secondly, the equivalent model of the diode is a simplified model, which does not take the ohmic loss into consideration. As the ECM of the diode is further improved by considering ohmic loss and optimizing the value of  $C_{diode}$ , the measurements and simulations reach a good agreement ( $R_d = 10 \Omega$ ,  $R_{OFF} = 2000 \Omega$ ), shown in Figure 10(b).

It is interesting to see that the AS does not cause any fluctuations in the transmission coefficient this time. Specifically, the  $S_{21}$  of the DUT2 with AS is larger than that without AS when the frequency is lower than 1.5 GHz while in the higher frequency range, the trend is opposite. Since the resonance mode of the AS varies with frequency, the  $S_{21}$  may be increased in some band but decreased in others.

In summary, the influence caused by AS on the transmission coefficient is not significant and less than 1 dB according to the measured results of DUT2. In addition, as the dimension of AS changed, the influence on transmission coefficient also varies when comparing the measured results of DUT1 and DUT2 together.

### High-power signal measurements

The transmission coefficient of MESS with and without AS for high-power signals are measured at 1.3 GHz, shown in Figure 11. For DUT1, the RT of the prototype with AS is about 1.2 kV/m while that without AS does not appear when the field intensity is less than 4.2 kV/m. For DUT2, the RT of the prototype with and without AS is about 1.2 kV/m and 6.5 kV/m, respectively. The results of both DUTs prove that the AS plays a critical role in the design of RT and the proposed method is useful in the MESS design.

### Comparison

To illustrate the advantages of the proposed method, the results of this paper are compared with the previous works, shown in the Table 1. In [19], the RT is designed by changing the geometry parameters of the unit cells, the RT of ESS becomes 1.3 times the initial value. In [18], the RT is designed by changing the types of diodes, and the variation range of RT is up to 10 times theoretically (no experiments in [18]). However, the change of diodes

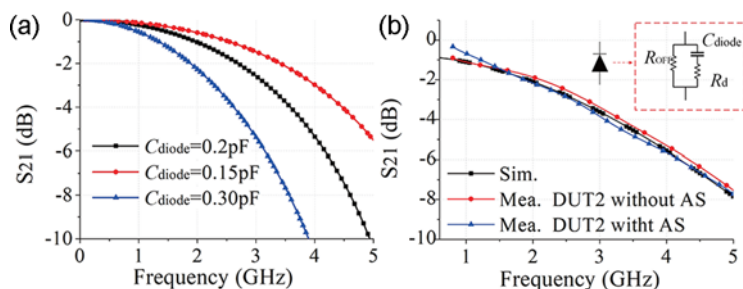


**Figure 10.** The analysis of the causes of errors. (a) The effects of capacitance and (b) the effects of the ECM of the diode.

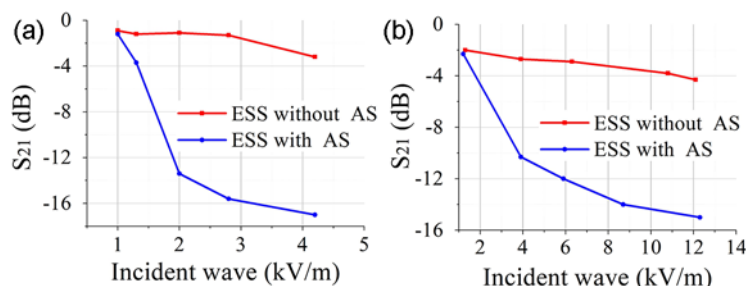


**Figure 11.** The transmission coefficient of two MESS prototypes with and without AS for high-power signals (a) DUT1 and (b) DUT2.

**Table 1.** Comparison of different methods

Ref	Working mechanism	Variation range of RT
This paper	Adding auxiliary structures	5 times
Ref. [19]	Changing the parameters of unit cell	1.3 times
Ref. [18]	Changing diodes	10 times

may significantly increase the cost and makes negative impacts on other indicators of ESS. For instance, if the diode of ESS is changed from a PIN diode to a Schottky diode, the power capacity will be reduced. Besides, the operating frequency, and the response time of ESS may also be changed with the diodes. On the contrary, the proposed method in this paper makes a noticeable design effect on the RT of ESS without introducing extra cost or negative impacts.

## Conclusion

In this paper, a detailed analysis of the RT of the SLC\_based\_ESS is presented. For demonstration, an ESS structure composed of metal strips and diodes is investigated. According to our research, the RT of MESS is rarely related to the geometry parameters of unit cell. However, the RT could be modulated by introducing AS into the MESS arrays. With the AS, the induced currents on diodes are enhanced and thus RT is greatly reduced. In addition, the AS only causes slight influence on the transmission performance of MESS. The results of simulations and experiments agree well, validating the proposed methods. The proposed method is not only useful for MESS but also can be applied to the design of other SLC\_based\_ESS structures.

**Funding statement.** This work was supported by the Hunan Provincial Natural Science Foundation of China (Yanlin Xu, Grant Number 2022JJ20045).

**Competing interests.** The authors report no conflict of interest.

## References

- Liu PG, Liu CX, Tan, JF, Dong, YF and Yi, B (2015) Analysis of the research development on HPM/EMP protection. *Chinese Journal of Ship Research* **10**(2), 2–6 (in Chinese).
- Eleftheriades GV (2014) Electronics protecting the weak from the strong. *Nature* **505**(7484), 490–491.
- Yang C, Brüns, H.-D, Schuster, C and Liu, PG (2016) Impulse response optimization of band-limited frequency data for hybrid field-circuit simulation of large-scale energy-selective diode grids. *IEEE Transactions on Electromagnetic Compatibility* **58**(4), 1072–1080.
- Yang C, Liu P and Huang X (2013) A novel method of energy selective surface for adaptive HPM/EMP protection. *IEEE Antennas and Wireless Propagation Letters* **12**(12), 112–115.
- Deng F, Xi XJ, Li J and Ding F (2015) Method of designing a field-controlled active frequency selective surface. *IEEE Antennas and Wireless Propagation Letters* **14**(2), 630–633.
- Chen Z, Chen X and Xu G (2017) A spatial power limiter using a nonlinear frequency selective surface. *International Journal of RF and Microwave Computer-Aided Engineering* **10**(253), 3265–3271.
- Chen Z, Wang CF and Aditya S (2019) Power-dependent frequency-selective surface: Concept, design, and experiment. *IEEE Transactions on Antennas and Propagation* **67**(5), 3215–3219.
- Monni S, Bekers DJ, van Wanum M, van Dijk R, Neto A, Gerini G and van Vliet FE (2009). Limiting frequency selective surfaces. Rome, Italy: IEEE. In *Proc. EuMC*. pp. 606–609.
- Hu N, Wang K, Zhang J, Zha S, Wu Z, Liu C and Liu P (2019) Design of ultrawideband energy-selective surface for high-power microwave protection. *IEEE Antennas and Wireless Propagation Letters* **18**(4), 669–673.
- Qin D and Zhang W (2019) Design of energy selective surfaces with wide reflection band. Shenzhen, China IEEE. In *2019 Computing, Communications and IoT Applications (ComComAp)*. pp. 425–427.
- Wall WS, Rudolph SM, Hong SK and Morgan KL (2014) Broadband switching nonlinear metamaterial. *IEEE Antennas and Wireless Propagation Letters* **12**(6), 427–430.
- Hu N, Liu YP, Xu H and Costa F (2022) High-performance energy selective surface based on equivalent circuit design approach. *IEEE Transactions on Antennas and Propagation* **70**(6), 4526–4538.
- Zhou L, Liu L and Shen Z (2021) High-performance energy selective surface based on the double-resonance concept. *IEEE Transactions on Antennas and Propagation* **69**(11), 7658–7666.

14. **Hu N, Zha S, Tian T and Liu P** (2022) Design and analysis of multiband energy selective surface based on semiconductors. *IEEE Transactions on Electromagnetic Compatibility* **64**(4), 1076–1085.
15. **Zhou Q, Liu P, Yu D, Bian L and Liu C** (2019) Field-controlled switchable frequency selective surface with broadband absorption characteristic. *IET Microwaves, Antennas & Propagation* **12**(9), 1470–1476.
16. **Zhang JH, Hu N, Wu, ZF, Deng, BW, Ding, L, Lin, MT and Liu, pg** (2021) A high-performance nonlinear metasurface for spatial-wave absorption. *IEEE Transactions on Antennas and Propagation* **69**(11), 7679–7687.
17. **Deng B, Lin M, Zhang J, Wu Z, Liu C and Liu P** (2021) PIN-diode-based high-intensity radiation fields (HIRF) protection of a printed dipole antenna. *IEEE Transactions on Electromagnetic Compatibility* **63**(1), 198–205.
18. **Yang C, Torbe W, De Marco S, Marc, Kopf and Christian, Schuster** (2021) Analysis and optimization of nonlinear diode grids for shielding of enclosures with apertures. *IEEE Transactions on Electromagnetic Compatibility* **63**(6), 300–312.
19. **Hu N, Liu C, Tian T, Xu Y and Liu P** (2023) Design and analysis of response threshold of energy selective surface based on diode grids. *IEEE Transactions on Electromagnetic Compatibility* **65**(2), 386–394.
20. **Costa F, Monorchio A and Manara G** (2012) Efficient analysis of frequency-selective surfaces by a simple equivalent-circuit model. *IEEE Transactions on Antennas and Propagation* **54**(4), 35–48.
21. **Marcuvitz N** (1951) *Waveguide Handbook*. McGraw-Hill Book Co.Inc, New York, USA.



**Ning Hu** received the B.S. degree in electronic engineering and the M.S. degree in electronic science and technology from National University of Defense Technology (NUDT), Changsha, Hunan, P.R. China, in 2017 and 2019, respectively. And he received the Ph.D. degree in information and communication engineering from NUDT in 2023. His research interests include electromagnetic compatibility and protection, metamaterials, and antennas.



**Xi Zhu** is currently a Lecture with the Information Engineering University. He received the Ph.D. degree in electronic science and technology from National University of Defense Technology in 2022. His current research interests include neuromorphic computing and simulation technology.



**He Wang** received the B.S. degree in computer science and technology from Zhengzhou University (ZZU) in 2018 and the M.S. degree in cybersecurity from Xidian University (XDU) in 2021. Her research interests include system security assessment.



**Haojie Yin** currently a tutor with the Information Engineering University. He received the Master's degree in Control Science and Engineering from Shandong University in 2023. His current research interests include simulation technology and data-driven modeling.



**Yanlin Xu** was born in Tianchang, Anhui, China, in 1990. He received the B.S. and M.S. degrees in electronic science and technology from National University of Defense Technology (NUDT), Changsha, China, in 2013 and 2015, respectively. And he received the Ph.D. degree in information and communication engineering from NUDT in 2018. His current research interests include electromagnetic compatibility and protection, computational electromagnetics, and its applications in scattering analysis.